universe

MDPI

Communication

Multi-Wavelength Properties of the 2021 Periastron Passage of PSR B1259-63

Maria Chernyakova [1,2,*], Denys Malyshev [3], Brian van Soelen [4], Shane O'Sullivan [1], Charlotte Sobey [5], Sergey Tsygankov [6,7], Samuel Mc Keague [1], Jacob Green [1], Matthew Kirwan [1], Andrea Santangelo [3], Gerd Pühlhofer [3] and Itumeleng M. Monageng [8,9]

1 School of Physical Sciences and Centre for Astrophysics & Relativity, Dublin City University, D09 W6Y4 Glasnevin, Ireland; shane.osullivan@dcu.ie (S.O.); samuel.mckeague2@mail.dcu.ie (S.M.K.); jacob.green7@mail.dcu.ie (J.G.); ma.kirwan32@mail.dcu.ie (M.K.)
2 Dublin Institute for Advanced Studies, 31 Fitzwilliam Place, D02 XF86 Dublin 2, Ireland
3 Institut für Astronomie und Astrophysik Tübingen, Universität Tübingen, Sand 1, D-72076 Tübingen, Germany; denys.malyshev@astro.uni-tuebingen.de (D.M.); andrea.santangelo@uni-tuebingen.de (A.S.); gerd.puehlhofer@astro.uni-tuebingen.de (G.P.)
4 Department of Physics, University of the Free State, P.O. Box 339, Bloemfontein 9300, South Africa; vansoelenb@ufs.ac.za
5 CSIRO Astronomy and Space Science, P.O. Box 1130, Bentley, WA 6102, Australia; charlotte.sobey@csiro.au
6 Department of Physics and Astronomy, University of Turku, FI-20014 Turku, Finland; sergey.tsygankov@utu.fi
7 Space Research Institute of the Russian Academy of Sciences, Profsoyuznaya Str. 84/32, 117997 Moscow, Russia
8 South African Astronomical Observatory, P.O. Box 9, Observatory, Cape Town 7935, South Africa; itu@saao.ac.za
9 Department of Astronomy, University of Cape Town, Private Bag X3, Rondebosch 7701, South Africa
* Correspondence: masha.chernyakova@dcu.ie

Citation: Chernyakova, M.; Malyshev, D.; van Soelen, B.; O'Sullivan, S.; Sobey, C.; Tsygankov, S.; Mc Keague, S.; Green, J.; Kirwan, M.; Santangelo, A.; et al. Multi-Wavelength Properties of the 2021 Periastron Passage of PSR B1259-63. *Universe* **2021**, *7*, 242. https://doi.org/10.3390/universe7070242

Academic Editor: Lucio Angelo Antonelli

Received: 10 June 2021
Accepted: 9 July 2021
Published: 13 July 2021

Abstract: PSR B1259-63 is a gamma-ray binary system hosting a radio pulsar orbiting around a O9.5Ve star, LS 2883, with a period of ∼3.4 years. The interaction of the pulsar wind with the LS 2883 outflow leads to unpulsed broadband emission in the radio, X-ray, GeV, and TeV domains. One of the most unusual features of the system is an outburst of GeV energies around the periastron, during which the energy release substantially exceeds the spin down luminosity under the assumption of the isotropic emission. In this paper, we present the first results of a recent multi-wavelength campaign (radio, optical, and X-ray bands) accompanied by the analysis of publicly available GeV *Fermi/LAT* data. The campaign covered a period of more than 100 days around the 2021 periastron and revealed substantial differences from previously observed passages. We report a major delay of the GeV flare, weaker X-ray flux during the peaks, which are typically attributed to the times when the pulsar crosses the disk, and the appearance of a third X-ray peak never observed before. We argue that these features are consistent with the emission cone model proposed by us previously, in the case of a sparser and clumpier disk of the Be star.

Keywords: gamma rays: general; pulsars: individual: PSR B1259-63; stars: emission-line, Be; X-rays: binaries; X-rays: individual: PSR B1259-63; radiation mechanisms: non-thermal

1. Introduction

PSR B1259-63 (PSR J1302–6350) is a 47.76-ms radio pulsar orbiting an O9.5Ve star (LS 2883) with a period of ∼1236.7 days in a highly eccentric orbit (e∼0.87) [1–3]. The Be stellar disk is highly inclined to the orbital plane [4], so that the pulsar crosses the disk twice per orbit. Based on the parallax data in the Gaia DR2 Archive [5] the distance to the system is 2.39 ± 0.19 kpc, which is consistent with the value of $2.6^{+0.4}_{-0.3}$ kpc reported previously [6]. PSR B1259-63 is one of two known systems where an interaction between the pulsar wind and the mass outflow from the young, massive companion leads to broadband (from radio

up to TeV energies), unpulsed non-thermal emission (see e.g., [7], and references therein). Another known pulsar with similar broadband properties, PSR J2032 + 4127, has an orbital period of about 50 years [8,9] and thus the possibilities to study the details of the interaction of the winds near the periastron in this system are very limited. The nature of the compact source in all other known gamma-ray binaries is not yet known. These systems can either harbour a hidden pulsar or a black hole (see e.g., [7] for a review), and thus detailed studies of PSR B1259-63 as a model system are highly important.

PSR B1259-63 was discovered in 1992 during the Parkes Galactic plane survey [1,10] as the first radio pulsar in orbit around an OB star. Further observations revealed that the pulsed radio emission is completely absorbed from around 20 days before to 20 days after periastron, but that unpulsed radio emission appears about 20 days before the periastron, quickly rising to a flux exceeding the pulsed flux by a factor of several tens, and shows two peaks that are associated with the pulsar crossing the plane of the circumstellar disk, before and after the periastron, and lasts for at least 100 hundred days after periastron [11,12]. In X-rays, PSR B1259-63 is visible throughout the whole orbit with two flux peaks approximately 15 days before and after periastron, similar to the radio light curve (see e.g., [13,14]).

During the periastron passage, PSR B1259-63 is also visible at high and very high energies (e.g., [15,16]). In 2010, 2014 and 2017, the light curve at GeV energies was marked by the presence of a strong flare, which occurred about 30–40 days after the periastron (e.g., [15,17,18]). In 2017, the flare was characterized by the presence of variability on timescales as short as 15 min, during which the energy release substantially exceeded the spin down luminosity (in the case of an isotropic outburst) by a factor of $\sim$30 [15,19]. These flares were observed only at GeV energies with no obvious counterparts at other wavelengths despite the possible link to a decrease of the Hα equivalent width [20,21]. To explain the luminosity of the GeV flare and the absence of counterparts at other wavelengths, a model was proposed [22] in which the TeV and X-ray emission is generated by the strongly accelerated electrons of the pulsar wind (IC and synchrotron emission correspondingly). The GeV emission in this model is a result of the IC emission of the unshocked and weakly shocked electrons, with a possible addition of bremsstrahlung emission on the clumps of the stellar wind material which penetrated beyond the shock cone. The unshocked electrons of the pulsar wind in this model are quasi-monochromatic, with energies of about 1 GeV. The luminosity of the GeV flares within this model can be understood if it is assumed that the initially isotropic pulsar wind after the shock is reversed and confined within a cone looking, during the flare, in the direction of the observer.

In order to test this model, we organised an intensive multi-wavelength campaign to follow the 2021 periastron passage of PSR B1259-63, which happened on MJD 59254.87/9 February 2021, in radio (ATCA), optical (SALT) and X-rays (*Swift*/XRT). Below we present the first results of this campaign, including the analysis of the GeV data as seen by the Large Area Telescope (LAT) on board the Fermi Gamma-ray Space Mission. In Section 2 of this paper, we describe the details of the observations and data analysis, in Section 3, we present our results, and we give our conclusions in Section 4.

2. Data Analysis

2.1. Radio Data

The Australia Telescope Compact Array (ATCA) was used to obtain the radio light curve of PSR B1259-63 from 19 February 2021 to 13 May 2021. The ATCA is a radio interferometer with six 22-m antennas providing a maximum baseline of 6 km, located in Narrabri, NSW, Australia. The observations of PSR B1259-63 were conducted in the 4-cm band using the Compact Array Broadband Backend (CABB) with centre frequencies of 5.5 GHz and 9 GHz, each with 2 GHz of bandwidth and 1 MHz frequency channels [23]. CABB was configured in a mode that allowed us to record the radio continuum and pulsar-binning data.

We observed PSR B1259-63 for 3 h approximately every 2 days (as allowed by the telescope schedule) across the above time period. The ATCA primary calibrator B1934-638 was observed for at least 10 min during each observation. We observed a secondary calibrator, J1322-6532, for 2 min for every 20 min on the target (i.e., PSR B1259-63). Here we report on the continuum data analysis at 5.5 GHz only. Later work will include a full analysis of the data at both centre frequencies, providing information on the spectral, polarization and Faraday rotation measure behavior of both the continuum emission and the pulsed emission.

The Miriad software was used for the data calibration and analysis, following standard routines [24]. The bandpass calibration and the absolute flux density calibration were done using B1934-638. The bandpass calibration was copied to the secondary (phase) calibrator, J1322-6532, which has an angular separation of 2.7 deg from the target. The J1322-6532 data were then used to calibrate the frequency-dependent complex gains and their time variations, as well as the instrumental polarization. Before copying these solutions to the target, the flux density of J1322-6532 was scaled to that of B1934-638. Flagging of radio frequency interference (RFI) and time-ranges with poor data quality was done in an iterative manner during the above process. The calibration routines described above were then repeated to obtain the final calibrated visibility data. Since the target is a point source at the phase centre, the 5.5 GHz flux density values were obtained using the mean visibility value reported by the Miriad task UVFLUX, with the uncertainty in this value obtained by dividing the quoted rms scatter in the visibilities by the square root of the number of correlations.

2.2. Optical Data

Spectroscopic observations were undertaken around periastron using the Southern African Large Telescope (SALT), with both the RSS and HRS spectrographs [25–27]. Between 22 days before, to 80 days after periastron, the source was observed 28 times with the RSS using the pg0900 and pg2300 grating, and 10 times with the HRS in Medium Resolution mode (R = 40,000). The RSS data was pre-reduced using the SALT pipeline, and flat correction, wavelength calibration and spectral extraction were performed using NUMPY/SCIPY/ASTROPY. The HRS observations were reduced using the pipeline presented in [28]. Individual spectra taken on the same night were averaged, continuum corrected and barycentric corrected. We report here on the change in the equivalent width of the Hα line, and future publications will present a more detailed analysis of the optical behavior. The equivalent width for each observation was measured multiple times, randomly shifting the wavelength range by $\pm$4 Å, and the median and standard deviation of the measurements obtained are reported as the value and uncertainty. The choice of continuum correction of the observations can introduce additional systematic offsets and we ensured that the continuum correction used results in the equivalent width measured with the RSS and HRS on 28 January 2021 ($\approx$12 days before periastron) having, within error, the value. The Hα equivalent width is shown in the lower panel of Figure 1.

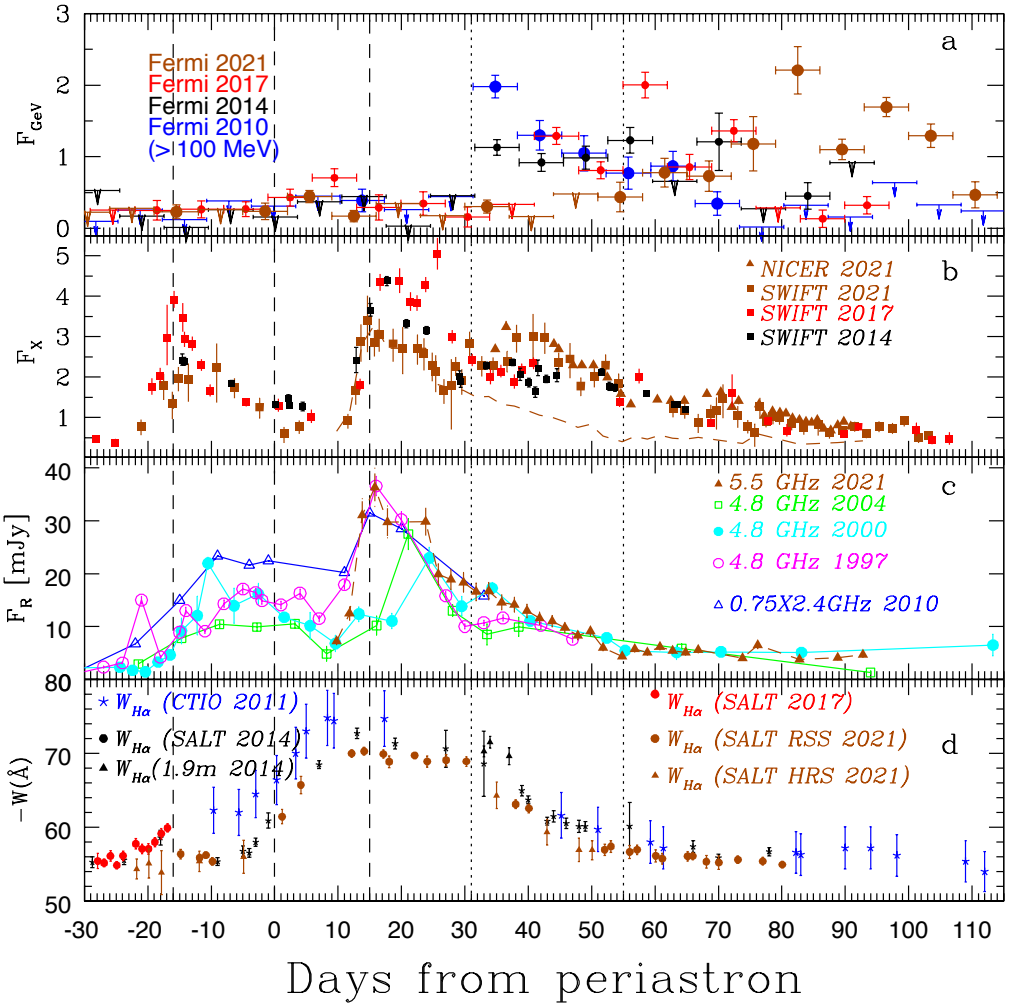

Figure 1. Evolution of PSR B1259-63 flux over the different periastron passages. Dashed lines correspond to the periastron and to the moments of disappearance (first non-detection) and reappearance (first detection) of the pulsed emission, as observed in 2010 [17]. Dotted lines correspond to the first appearance of the detection in GeV band at a day time scale in 2010 and 2021. (**a**) *Fermi/LAT* flux measurements in the E > 100 MeV energy range with a weekly bin size. Flux is given in 10^{-6} cm^{-2} s^{-1}. (**b**) absorbed 1–10 keV X-ray flux in units of 10^{-11} erg cm^{-2} s^{-1}. Scaled 5.5-GHz radio data from 2021 are also shown in this panel with a gold dashed line for comparison. (**c**) radio flux densities in mJy. Radio data for the years 1997, 2000 and 2004 are taken from [12]. Radio data from 2010 are taken from [17] and are normalized by a factor 0.75. Please note that data from different years are taken at different frequencies. (**d**) H α equivalent width. Data from 2011 are taken from [20], and 2014 and 2017 data are taken from [22].

2.3. X-ray Data

2.3.1. *Swift*/XRT

A full overview of the X-ray flux for the SWIFT observations around the years 2014, 2017 and 2021 are presented in the panel (b) of Figure 1. Historical data in this figure are taken from [22]. The 2021 periastron passage of PSR B1259-63 was closely monitored by the *Swift* satellite [29]. We have analyzed all available data taken from 19 January 2021 to 24 May 2021. The data was reprocessed and analysed as suggested by the *Swift*/XRT team[1] with the `xrtpipeline v.0.13.5` and `heasoft v.6.28` software package. The spectral analysis of *Swift*/XRT spectra was performed with `XSPEC v.12.11.1`. The spectrum was extracted from a circle of radius 36″ around the position of PSR B1259-63, and the background estimated from a co-centred annulus with inner/outer radii of 60″/300″. We performed the

fit of the spectrum, grouped to have at least 1 photon per energy bin using cash statistic [30] by an absorbed powerlaw model (`cflux*tbabs*po`) in 0.3–10 keV range. The flux of the source, hydrogen column density and the slope of the powerlaw were treated as free parameters during the fit. The uncertainties of *Swift*/XRT flux shown in Figure 1 are 1σ c.r.

2.3.2. NICER

About 35 days after the periastron passage, the *NICER* instrument [31] started to monitor PSR B1259-63's evolution. The *NICER* data was reduced using the NICERDAS software version 2020-04-23_V007a with default filtering criteria applied. The background was estimated using the *NICER* tool NIBACKGEN3C50[2] (Remillard et al., in prep.) with the default parameters. The spectra obtained for each observation were binned to have at least 1 count per energy bin, and cash statistic [30,32][3] was applied while fitting the data in the 0.5–10 keV energy range. The relatively high background level (around 20–30% of the total count rate detected from PSR B1259-63) did not allow us to determine the spectral photon index reliably, which is strongly affected by the quality of the background subtraction. Therefore, in order to estimate flux from the source we fixed the photon index at an averaged value of 1.5, obtained from the *Swift*/XRT data.

2.4. Gamma-Ray Data

The analysis of *Fermi/LAT* data was performed using Fermitools version 2.0.8 (released 20 January 2021). For the analysis of the 2021 periastron passage and the combined periastron data, the analysis was carried out using the latest Pass 8 reprocessed data (P8R3) from the CLEAN event class. The binned likelihood analysis was performed for photons within the energy range 0.1–100 GeV that arrived between 1 January 2021 and 6 June 2021 within a 20°-radius region around PSR B1259-63's position. The selected maximum zenith angle was 90°. The performed analysis relies on the fitting of the spectral and spatial model of the region to the observed data in a series of energy and time bins.

The adapted model of the region included templates for the Galactic and isotropic diffuse emission components provided by *Fermi/LAT* collaboration, as well as all sources from the latest 4FGL-DR2 *Fermi/LAT* catalogue [33], with the spectral templates selected according to the catalogue. At the initial stage of the analysis we assumed all spectral parameters of sources within 15° around PSR B1259-63 to be free parameters and fixed all spectral parameters of sources between 15° and 20° to their catalogue values. We performed the fitting of the described model to the whole available data-set. For the subsequent analysis, we fixed all (except normalisations) free spectral parameters to their best-fit values, and removed all of the weak sources detected with test-statistics $TS < 1$ from the model.

At the next step of the analysis, we split the 0.1–10 GeV data over a series of 1-day and 1-week bins aiming to produce the light curve of PSR B1259-63 in the corresponding energy band, see Figure 2, left panel. All upper limits presented were calculated using the IntegralUpperLimits module included in fermitools for $TS < 4$ cases and correspond to a 95% confidence level.

The obtained light curve suggests the enhancement of the GeV emission during 55–108 days (MJD 59310–59363) after the periastron. Below we refer to this period as "*Fermi/LAT* flare" during the 2021 periastron passage. To study the potential spectral-shape variability of the source during different periods of the 2021 periastron passage, we built the spectrum of PSR B1259-63 for the periods $(-20; 0)$, $(0; +20)$ days around the periastron, as well as during the *Fermi/LAT* flare period. Resulting spectra are shown in Figure 3. The best-fit spectral parameters in *Fermi/LAT* band as well as the suggested for the fit model are summarized in Table 1.

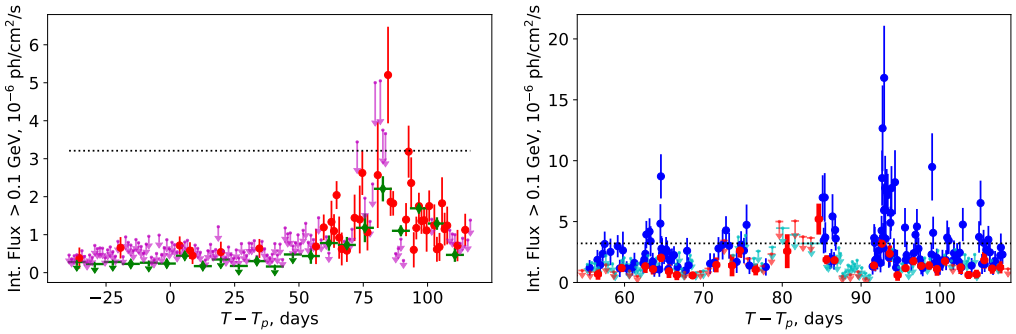

Figure 2. (**Left**) *Fermi/LAT* weekly (green points) and daily (magenta upper limits and red points–detection's with $TS > 4$) light curves of PSR B1259-63 at energies 0.1–10 GeV. The dotted line represents the flux corresponding to spin-down luminosity of PSR B1259-63 ($L_{sd} = 8.2 \times 10^{35}$ erg/s). (**Right**) Blue points and cyan upper limits: *Fermi/LAT* light curve at >0.1 GeV range for the period MJD 59310–59363 ((+55; +108) days after the periastron) with adaptive time binning (to have 9 photons per time bin in 1° radius circle around PSR B1259-63 position at 0.1–10 GeV). The light curve covers the period of the highest flux of the source in the GeV band. Red points correspond to a daily light curve, same as in the left panel. See text for the details.

For the period of the 2021 *Fermi/LAT* flare we performed dedicated studies for a short timescale ($\ll$1 day) variability aiming to identify bright sub-flares known to be present during the 2017 periastron passage. We split the whole time range of *Fermi/LAT* flare over a set of variable-length time bins, such that each time bin accommodates 9 photons with energies 0.1–10 GeV in 1°-radius circle around PSR B1259-63 position. The resulted time bins have durations from 5 min to 2.8 days with an average duration of ∼6 h. For each of the time bins we extracted the flux of PSR B1259-63 in a way similar to one which was used for daily/weekly GeV light curve production. To produce short timescale light curve we explicitly set the spectral model of PSR B1259-63 to be a (super-exponential)cutoff powerlaw with the indexes and cutoff energy fixed to their best-fit values observed during *Fermi/LAT* 2021 flare, see Table 1. The obtained light curve is shown in Figure 2, right panel.

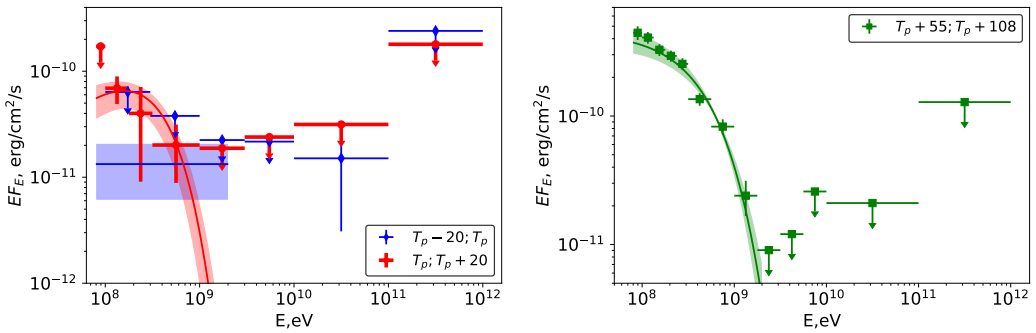

Figure 3. (**Left**) *Fermi/LAT* spectra of PSR B1259-63 as seen at (−20–0) days before the periastron 2021 (blue points) and (0–+20) days after the periastron 2021 (red points). Shaded regions of the corresponding color illustrate 1σ confidence range for the fitted models. (**Right**) *Fermi/LAT* spectrum of the period characterized by the highest flux in >0.1 GeV band during 2021 periastron passage (+55–+108 days after the periastron), see Table 1 for the best-fit parameters' values.

Table 1. The best-fit parameters of the models (PL–power law or SECPL–super-exponential cutoff power law with exponent index β) used to fit *Fermi/LAT* data during different periods of the 2021 periastron passage in 0.08–2 GeV energy band. See text and Figure 3 for the details.

Period Days	Model	Norm at 1 GeV 10^{-9} ph/cm^2/s	Index	Cutoff GeV	β	TS
$(-20; 0)$	PL	0.6 ± 0.3	2 (*fixed*)	–	–	7
$(0; +20)$	SECPL	0.5 ± 0.2	1.1 ± 0.2	0.18 ± 0.03	1(*fixed*)	48
$(+55; +108)$	SECPL	0.31 ± 0.002	1.97 ± 0.01	0.38 ± 0.01	0.96 ± 0.01	1373
$(-40; +116)$	PL	$(1.47 \pm 0.01) \times 10^{-2}$	2.70 ± 0.01	–	–	600

3. Results and Discussion

The 2021 periastron passage of PSR B1259-63 is marked by very unusual behaviour both in X-rays and the GeV band. While the rise of the X-ray emission during the first and second disk crossing is similar to that observed during previous periastron passages, the heights of these two peaks are substantially smaller (see panel (b) of Figure 1). We note that the observations of PSR B1259-63 in 2021 allow usto estimate the characteristic rise time of the X-ray emission during these episodes to be as short as $\sim$1 day, which indicates that the Be star's disk is characterized by high-density gradients. Most interestingly, the 2021 X-ray light curve shows a third peak, which starts to rise $\approx$30 days after periastron. This rise occurs at approximately the same time as the GeV flare in 2010 and 2014. Such X-ray behavior was never observed during previous periastra passages and has no clear counterparts at any other wavelengths.

The 2021 radio observations demonstrate a strong correlation with the second X-ray peak during the period between 10 and 28 days after the periastron. To better illustrate this point, we plot the re-scaled radio data on panel (b) of Figure 1 (dashed line). With the rise of the third X-ray peak this correlation disappears. At the same time, the 2021 radio observations seem to be consistent with previous observations at 4.8 GHz [11,12].

The GeV emission in 2021 is marked by a large delay in the rise of the flux. At early phases (-20 to 0 and 0 to +20 days from periastron) the spectral characteristics of PSR B1259-63 in the GeV band are consistent with the average values in 2011-2017 reported in [22], see Figure 3. However, contrary to previous passages, up to 55 days after periastron, the flux (>0.1 GeV) remained at a level of $(0.2 - 0.4) \times 10^{-6}$ ph/cm^2/s, which is consistent with the flux observed before the periastron passage.

The period of 55–108 days after the periastron was marked by a rise of the GeV flux up to the level $\sim 2 \times 10^{-6}$ ph/cm^2/s on weekly timescales comparable to the values observed during the flare period in 2010 and 2017, and twice as high as than in 2014 (see top panel of Figure 1). Similar to previous periastron passages [22], the GeV spectrum during this period was well described by a super-exponential cut-off power-law model (see Table 1 and the right panel of Figure 3). After this period the *Fermi/LAT* light curve is characterized by a gradual decay of the flux.

Regular observations using SALT during 2021 provided the most frequent observations yet obtained, from 22 days before to 80 days after periastron. Given the marked difference of X-ray and GeV behavior of the source during periastron 2021, the optical observations were, remarkably, very closely aligned with previous observations. A comparison to the behavior in 2014 shows a slightly weaker equivalent width during 2021. There does appear to be a slightly lower equivalent width around 30–50 days after periastron, compared to the 2014 periastron when the GeV gamma-ray flux was higher (although the uncertainties in the 2014 observations over this period are larger). While the peak in the GeV activity occurs after 80 days after periastron, the equivalent width showed no dramatic change following the onset of increased GeV activity, 50 days after periastron, despite the large difference in the GeV gamma-ray activity compared to previous periastra. The decrease in the equivalent width from 40 days after periastron onward, appears to be consistent with that observed in 2010 and 2014, when the GeV gamma-ray activity was decreasing. This indicates the limits in using the Hα to directly trace the GeV behavior as

suggested by [21,34]. The increased gamma-ray activity has occurred much later during 2021, at a larger binary separation (2.6 AU, 4 AU, and 5 AU at 30 days, 55 days and 80 days after periastron, respectively) and the region of the circumstellar disk producing the H α emission may be far less affected during this periastron. Future observations at at longer wavelengths (infrared to millimeter) may be able to trace the disk's behavior at later orbital phases (see e.g., [35,36] and references therein).

Following the model proposed by [22] we suggest that the X-ray, GeV and TeV emission is generated within the "emission cone" formed by the interaction of the pulsar/Be star outflows. Be stars are well known to have highly variable outflows, sometimes even switching to a disc-less state, see reviews in [37,38]

The lower peak X-ray flux during the disk crossings, as well as the slightly lower H α equivalent width, may indicate that the Be star's circumstellar disk was less dense in 2021, which results in the stand-off shock being further from the pulsar and, consequently, a weaker magnetic field in the emission region. The sparser state of the Be star disk during 2021 periastron passage, along with likely a less dense polar outflow, results in a much larger opening angle of the emission cone than what was observed during previous periastron passages.

The third peak of the X-ray emission can be interpreted as originating from the presence of a large number of clumps above/below the disk (see right panel of Figure 4). Such clumps can substantially modify the smooth flow of the strongly shocked relativistic electrons along the emission cone's surface. This effectively increases their escape time from the system and leads to the enhanced level of X-ray emission. The GeV emission in the model of [22] is connected to the emission from the unshocked electrons of the pulsar wind. These electrons propagate mainly in the inner regions of the emission cone and are thus not significantly affected by the presence of clumps.

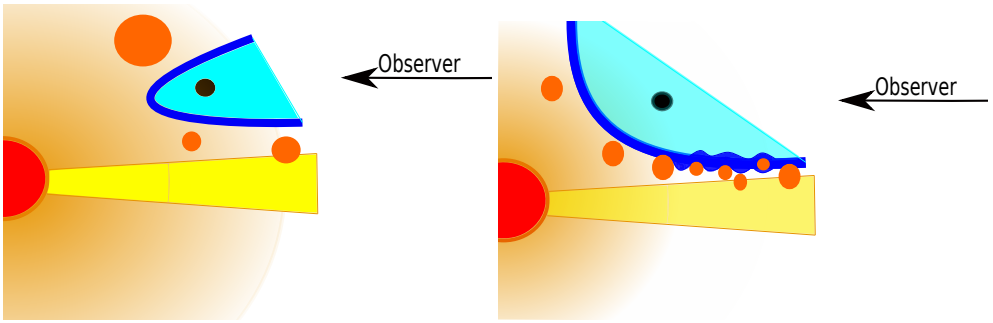

Figure 4. Schematic sketch of the 2017 (**left**) and 2021 (**right**) periastron passages. The positions of the star and the pulsar are shown with red and black circles, respectively. The equatorial stellar disk is depicted by the yellow shaded regions. The orange shaded regions and the orange circles depict the polar outflow and the clumps in the Be star's disk, respectively. The cyan regions correspond to the unshocked electrons of the pulsar wind. The blue region corresponds to the border of the emission cone along which strongly/weakly shocked electrons of the pulsar wind are leaving the system (see text for more details). All lengths in the figure are not to scale.

The peak level of the GeV emission in the discussed model is **inversely** proportional to the cone opening angle, which naturally explains the relatively low average flux level seen by *Fermi/LAT*, see Figure 2 (right panel) at shortest time scales. While at 1 day time scale the highest observed GeV flux at a level of 5×10^{-6} ph/cm^2/s is comparable to the level of similar flares seen after the 2017 periastron, we would like to note the substantial difference of the flux variability on intra-day timescales during the 2021 and 2017 passages. In 2017, PSR B1259-63 demonstrated variability on much shorter (15 min–3 h) timescales, with the flux exceeding the 1 day average by a factor up to 30 for 15 min flares [15]. During the current periastron passage, the source also showed a number of outbursts on a short time scale (5 min–3 h), with a flux $\sim 18 \times 10^{-6}$ ph/cm^2/s, see Figure 2. Although such outbursts require the luminosity of the source to be at a level of 4.6×10^{36} erg/s which exceeds the

spin-down luminosity (assuming $L_{sd} = 8.2 \times 10^{35}$ erg/s) of PSR B1259-63 by a factor of ∼5–6, this factor is significantly smaller than the factor of ∼30 required to explain the short-term variability of PSR B1259-63 seen in 2017. We therefore argue that the observed short timescale variability, within the model of [22], is consistent with a large ($\sim\pi$) opening angle of the emission cone.

The 1 day GeV-band light curve shown in the Figure 2 additionally indicates flux variability on 0.5–2 days timescales. The observed variability of GeV emission at short (few minutes–few days) time scales in the model of [22] can be explained by bremsstrahlung emission from the clumps of the Be star wind entering the emission cone. In this case, the variability timescale corresponds either to the characteristic size of a clump (e.g., shortest time scales) or to the lifetime of smaller clumps in the system (e.g., longest time scales).

In addition to the rapid flares caused by bremsstrahlung, some level of slowly time-varying GeV emission can originate from IC emission of weakly shocked electrons of the pulsar wind. A similar origin was proposed by [22] to explain the average GeV flare during the 2017 passage.

4. Conclusions

In this paper, we present the first results from intensive multi-wavelength observations of the 2021 periastron passage of PSR B1259-63. This periastron was marked by a number of unique features, namely:

- A lower X-ray flux during the periods of pre- and post-periastron disk crossings.
- The presence of a third X-ray flux peak starting about 30 days after the periastron.
- A correlation between the X-ray and radio fluxes during the second X-ray peak, and an absence of such a correlation with the third rise of the X-ray flux.
- A substantial delay in the rise of the GeV emission, which started only 55 days after the periastron.
- A surprising similarity in the variability of the H_α equivalent width compared to previous periastra passages.

We argue that the observed properties can be explained within the model of [22] under the assumption that the outer parts of the Be star's disk are characterized by lower densities (in comparison to previous periastron passages). We encourage IR observations of this system during the next periastron passages, as the state of the outer parts of the disk is poorly traced by the H_α line variability.

A more detailed analysis of the multi-wavelength data from this periastron passage is currently ongoing and will be the subject of an upcoming publication.

Author Contributions: Radio data observations and analysis, C.S., S.O., S.M.K., J.G., M.K.; optical data analysis, B.v.S. and I.M.M.; X-ray data analysis D.M. and S.T.; GeV data analysis, D.M.; PI of SALT observations, B.v.S.; PI of radio and X-ray proposals, M.C.; writing, M.C., D.M., B.v.S., S.O.; writing—review and editing, A.S., G.P., S.M.K., J.G., M.K. All authors have read and agreed to the published version of the manuscript.

Funding: S.M.K. was funded by ESA Prodex grant C4000120711. JG acknowledge financial support of CfAR. DM work was supported by DFG through the grant MA 7807/2-1 and DLR through the grant 50OR2104. ST acknowledges financial support by the grant 14.W03.31.0021 of the Ministry of Science and Higher Education of the Russian Federation.

Institutional Review Board Statement: Not applicable.

Informed Consent Statement: Not applicable.

Data Availability Statement: X-ray and GeV data are available in a publicly accessible repository. Radio and optical data are available on request.

Acknowledgments: We acknowledge the use of public data from the Swift data archive and thanks the entire Swift team for accepting and planning Target-of-Opportunity requests. This work made use of data supplied by the UK Swift Science Data Centre at the University of Leicester. This paper uses observations made at the South African Astronomical Observatory (SAAO). This paper uses

observation Some of the observations reported in this paper were obtained with the Southern African Large Telescope (SALT) under program 2018-1-MLT-002 (PI: B. van Soelen). The Australia Telescope Compact Array is part of the Australia Telescope National Facility which is funded by the Australian Government for operation as a National Facility managed by CSIRO. We acknowledge the Gomeroi people as the traditional owners of the Observatory site. The authors acknowledge support by the state of Baden-Württemberg through bwHPC.

Conflicts of Interest: The authors declare no conflict of interest. The funders had no role in the design of the study; in the collection, analyses, or interpretation of data; in the writing of the manuscript, or in the decision to publish the results.

Notes

1 https://swift.gsfc.nasa.gov/analysis/xrt_swguide_v1_2.pdf (accessed on 12 July 2021).
2 https://heasarc.gsfc.nasa.gov/docs/nicer/tools/nicer_bkg_est_tools.html (accessed on 12 July 2021).
3 https://heasarc.gsfc.nasa.gov/xanadu/xspec/manual/XSappendixStatistics.html (accessed on 12 July 2021).

References

1. Johnston, S.; Manchester, R.N.; Lyne, A.G.; Bailes, M.; Kaspi, V.M.; Qiao, G.; D'Amico, N. PSR 1259-63–A binary radio pulsar with a Be star companion. *Astrophys. J. Lett.* **1992**, *387*, L37–L41. [CrossRef]
2. Negueruela, I.; Okazaki, A.T.; Fabregat, J.; Coe, M.J.; Munari, U.; Tomov, T. The Be/X-ray transient 4U 0115+63/V635 Cassiopeiae. II. Outburst mechanisms. *Astron. Astrophys.* **2001**, *369*, 117–131. [CrossRef]
3. Shannon, R.M.; Johnston, S.; Manchester, R.N. The kinematics and orbital dynamics of the PSR B1259-63/LS 2883 system from 23 yr of pulsar timing. *Mon. Not. RAS* **2014**, *437*, 3255–3264. [CrossRef]
4. Wang, N.; Johnston, S.; Manchester, R.N. 13 years of timing of PSR B1259-63. *Mon. Not. RAS* **2004**, *351*, 599–606. [CrossRef]
5. Gaia Collaboration; Brown, A.G.A.; Vallenari, A.; Prusti, T.; de Bruijne, J.H.J.; Babusiaux, C.; Bailer-Jones, C.A.L.; Biermann, M.; Evans, D.W.; Eyer, L.; et al. Gaia Data Release 2. Summary of the contents and survey properties. *Astron. Astrophys.* **2018**, *616*, A1. [CrossRef]
6. Miller-Jones, J.C.A.; Deller, A.T.; Shannon, R.M.; Dodson, R.; Moldón, J.; Ribó, M.; Dubus, G.; Johnston, S.; Paredes, J.M.; Ransom, S.M.; et al. The geometric distance and binary orbit of PSR B1259-63. *arXiv* **2018**, arXiv:astro-ph.HE/1804.08402.
7. Chernyakova, M.; Malyshev, D. Gamma-ray binaries. In Proceedings of the Multifrequency Behaviour of High Energy Cosmic Sources–XIII, Palermo, Italy, 3–8 June 2019; p. 45.
8. Ho, W.C.G.; Ng, C.Y.; Lyne, A.G.; Stappers, B.W.; Coe, M.J.; Halpern, J.P.; Johnson, T.J.; Steele, I.A. Multiwavelength monitoring and X-ray brightening of Be X-ray binary PSR J2032+4127/MT91 213 on its approach to periastron. *Mon. Not. RAS* **2017**, *464*, 1211–1219. [CrossRef]
9. Chernyakova, M.; Malyshev, D.; Blay, P.; van Soelen, B.; Tsygankov, S. Multiwavelength observations of PSR J2032+4127 during the 2017 periastron passage. *Mon. Not. RAS* **2020**, *495*, 365–374. [CrossRef]
10. Johnston, S.; Lyne, A.G.; Manchester, R.N.; Kniffen, D.A.; D'Amico, N.; Lim, J.; Ashworth, M. A high-frequency survey of the southern Galactic plane for pulsars. *Mon. Not. RAS* **1992**, *255*, 401–411. [CrossRef]
11. Connors, T.W.; Johnston, S.; Manchester, R.N.; McConnell, D. The 2000 periastron passage of PSR B1259-63. *Mon. Not. RAS* **2002**, *336*, 1201–1208. [CrossRef]
12. Johnston, S.; Ball, L.; Wang, N.; Manchester, R.N. Radio observations of PSR B1259-63 through the 2004 periastron passage. *Mon. Not. RAS* **2005**, *358*, 1069–1075. [CrossRef]
13. Chernyakova, M.; Neronov, A.; Lutovinov, A.; Rodriguez, J.; Johnston, S. XMM-Newton observations of PSR B1259-63 near the 2004 periastron passage. *Mon. Not. RAS* **2006**, *367*, 1201–1208. [CrossRef]
14. Chernyakova, M.; Neronov, A.; Aharonian, F.; Uchiyama, Y.; Takahashi, T. X-ray observations of PSR B1259-63 near the 2007 periastron passage. *Mon. Not. RAS* **2009**, *397*, 2123–2132. [CrossRef]
15. Johnson, T.J.; Wood, K.S.; Kerr, M.; Corbet, R.H.D.; Cheung, C.C.; Ray, P.S.; Omodei, N. A Luminous and Highly Variable Gamma-Ray Flare Following the 2017 Periastron of PSR B1259-63/LS 2883. *Astrophys. J.* **2018**, *863*, 27. [CrossRef]
16. Abdalla, H.; Adam, R.; Aharonian, F.; Ait Benkhali, F.; Angüner, E.O.; Arakawa, M.; Arcaro, C.; Armand, C.; Ashkar, H.; Backes, M.; et al. H.E.S.S. and Fermi-LAT observations of PSR B1259-63/LS 2883 during its 2014 and 2017 periastron passages. *Astron. Astrophys.* **2020**, *633*, A102.
17. Abdo, A.A.; Ackermann, M.; Ajello, M.; Allafort, A.; Ballet, J.; Barbiellini, G.; Bastieri, D.; Bechtol, K.; Bellazzini, R.; Berenji, B.; et al. Discovery of High-energy Gamma-ray Emission from the Binary System PSR B1259-63/LS 2883 around Periastron with Fermi. *Astrophys. J. Lett.* **2011**, *736*, L11. [CrossRef]
18. Caliandro, G.A.; Cheung, C.C.; Li, J.; Scargle, J.D.; Torres, D.F.; Wood, K.S.; Chernyakova, M. Gamma-Ray Flare Activity from PSR B1259-63 during 2014 Periastron Passage and Comparison to Its 2010 Passage. *Astrophys. J.* **2015**, *811*, 68. [CrossRef]
19. Tam, P.H.T.; He, X.; Sarathi Pal, P.; Cui, Y. The hour-timescale GeV flares of PSR B1259-63 in 2017. *arXiv* **2018**, arXiv:1804.09861.

20. Chernyakova, M.; Abdo, A.A.; Neronov, A.; McSwain, M.V.; Moldón, J.; Ribó, M.; Paredes, J.M.; Sushch, I.; de Naurois, M.; Schwanke, U.; et al. Multiwavelength observations of the binary system PSR B1259-63/LS 2883 around the 2010-2011 periastron passage. *Mon. Not. RAS* **2014**, *439*, 432–445. [CrossRef]
21. Chernyakova, M.; Neronov, A.; van Soelen, B.; Callanan, P.; O'Shaughnessy, L.; Babyk, I.; Tsygankov, S.; Vovk, I.; Krivonos, R.; Tomsick, J.A.; et al. Multi-wavelength observations of the binary system PSR B1259-63/LS 2883 around the 2014 periastron passage. *Mon. Not. RAS* **2015**, *454*, 1358–1370. [CrossRef]
22. Chernyakova, M.; Malyshev, D.; Mc Keague, S.; van Soelen, B.; Marais, J.P.; Martin-Carrillo, A.; Murphy, D. New insight into the origin of the GeV flare in the binary system PSR B1259-63/LS 2883 from the 2017 periastron passage. *Mon. Not. RAS* **2020**, *497*, 648–655. [CrossRef]
23. Wilson, W.E.; Ferris, R.H.; Axtens, P.; Brown, A.; Davis, E.; Hampson, G.; Leach, M.; Roberts, P.; Saunders, S.; Koribalski, B.S.; et al. The Australia Telescope Compact Array Broad-band Backend: description and first results. *Mon. Not. RAS* **2011**, *416*, 832–856. [CrossRef]
24. Sault, R.J.; Teuben, P.J.; Wright, M.C.H. A Retrospective View of MIRIAD. In Proceedings of the Astronomical Data Analysis Software and Systems IV, Baltimore, MD, USA, 25–28 September 1994; Shaw, R.A., Payne, H.E., Hayes, J.J.E., Eds.; Astronomical Society of the Pacific Conference Series; NASA: Washington, DC, USA, 1995; Volume 77, p. 433.
25. Buckley, D.A.H.; Swart, G.P.; Meiring, J.G. Completion and commissioning of the Southern African Large Telescope. In Proceedings of the Society of Photo-Optical Instrumentation Engineers (SPIE) Conference Series, Orlando, FL, USA, 24–31 May 2006; Volume 6267, p. 62670Z. [CrossRef]
26. Burgh, E.B.; Nordsieck, K.H.; Kobulnicky, H.A.; Williams, T.B.; O'Donoghue, D.; Smith, M.P.; Percival, J.W. Prime Focus Imaging Spectrograph for the Southern African Large Telescope: Optical design. In Proceedings of the Instrument Design and Performance for Optical/Infrared Ground-based Telescopes, Society of Photo-Optical Instrumentation Engineers (SPIE) Conference Series, Waikoloa, HI, USA, 22–28 August 2003; Volume 4841, pp. 1463–1471. [CrossRef]
27. Bramall, D.G.; Sharples, R.; Tyas, L.; Schmoll, J.; Clark, P.; Luke, P.; Looker, N.; Dipper, N.A.; Ryan, S.; Buckley, D.A.H.; et al. The SALT HRS spectrograph: Final design, instrument capabilities, and operational modes. In Proceedings of the Ground-based and Airborne Instrumentation for Astronomy III, San Diego, CA, USA, 27 June–2 July 2010; McLean, I.S., Ramsay, S.K., Takami, H., Eds.; Society of Photo-Optical Instrumentation Engineers (SPIE) Conference Series; SPIE: Bellingham, WA, USA, 2010; Volume 7735, p. 77354F. [CrossRef]
28. Kniazev, A.Y.; Gvaramadze, V.V.; Berdnikov, L.N. MN48: A new Galactic bona fide luminous blue variable revealed by Spitzer and SALT. *Mon. Not. RAS* **2016**, *459*, 3068–3077. [CrossRef]
29. Gehrels, N.; Chincarini, G.; Giommi, P.; Mason, K.O.; Nousek, J.A.; Wells, A.A.; White, N.E.; Barthelmy, S.D.; Burrows, D.N.; Cominsky, L.R.; et al. The Swift Gamma-Ray Burst Mission. *Astrophys. J.* **2004**, *611*, 1005–1020. [CrossRef]
30. Cash, W. Parameter estimation in astronomy through application of the likelihood ratio. *Astrophys. J.* **1979**, *228*, 939–947. [CrossRef]
31. Gendreau, K.C.; Arzoumanian, Z.; Okajima, T. The Neutron star Interior Composition ExploreR (NICER): An Explorer mission of opportunity for soft X-ray timing spectroscopy. In Proceedings of the Space Telescopes and Instrumentation 2012: Ultraviolet to Gamma Ray, Amsterdam, The Netherlands, 1–6 July 2012; Takahashi, T., Murray, S.S., den Herder, J.W.A., Eds.; Society of Photo-Optical Instrumentation Engineers (SPIE) Conference Series; SPIE: Bellingham, WA, USA, 2012; Volume 8443, p. 844313. [CrossRef]
32. Wachter, K.; Leach, R.; Kellogg, E. Parameter estimation in X-ray astronomy using maximum likelihood. *Astrophys. J.* **1979**, *230*, 274–287. [CrossRef]
33. Abdollahi, S.; Acero, F.; Ackermann, M.; Ajello, M.; Atwood, W.B.; Axelsson, M.; Baldini, L.; Ballet, J.; Barbiellini, G.; Bastieri, D.; et al. Fermi Large Area Telescope Fourth Source Catalog. *Astrophys. J. Suppl.* **2020**, *247*, 33. [CrossRef]
34. Chernyakova, M.; Babyk, I.; Malyshev, D.; Vovk, I.; Tsygankov, S.; Takahashi, H.; Fukazawa, Y. Study of orbital and superorbital variability of LSI +61° 303 with X-ray data. *Mon. Not. RAS* **2017**, *470*, 1718–1728. [CrossRef]
35. Klement, R.; Carciofi, A.C.; Rivinius, T.; Matthews, L.D.; Vieira, R.G.; Ignace, R.; Bjorkman, J.E.; Mota, B.C.; Faes, D.M.; Bratcher, A.D.; et al. Revealing the structure of the outer disks of Be stars. *Astron. Astrophys.* **2017**, *601*, A74. [CrossRef]
36. Fujita, Y.; Nagai, H.; Kawachi, A.; Okazaki, A.T. ALMA Observations of PSR B1259-63/LS 2883 in an Inactive Period: Variable Circumstellar Disk? *arXiv* **2020**, arXiv:2005.00017.
37. Reig, P. Be/X-ray binaries. *Astrophys. Space Sci.* **2011**, *332*, 1–29. [CrossRef]
38. Porter, J.M.; Rivinius, T. Classical Be Stars. *Publ. ASP* **2003**, *115*, 1153–1170. [CrossRef]